First detection of solar neutrinos from the CNO cycle with Borexino

Gioacchino Ranucci
INFN - Milano

Borexino Collaboration

Virtual Free Meson Seminars @ DTP-TIFR Mumbay

March 25, 2021

The Borexino detector @ Gran Sasso

Active volume 280 tons of liquid scintillator

Detection principle

$$\nu_x + e \rightarrow \nu_x + e$$

Elastic scattering off the electrons of the scintillator threshold at ~ 60 keV (electron energy)

Data taking started in May 2007

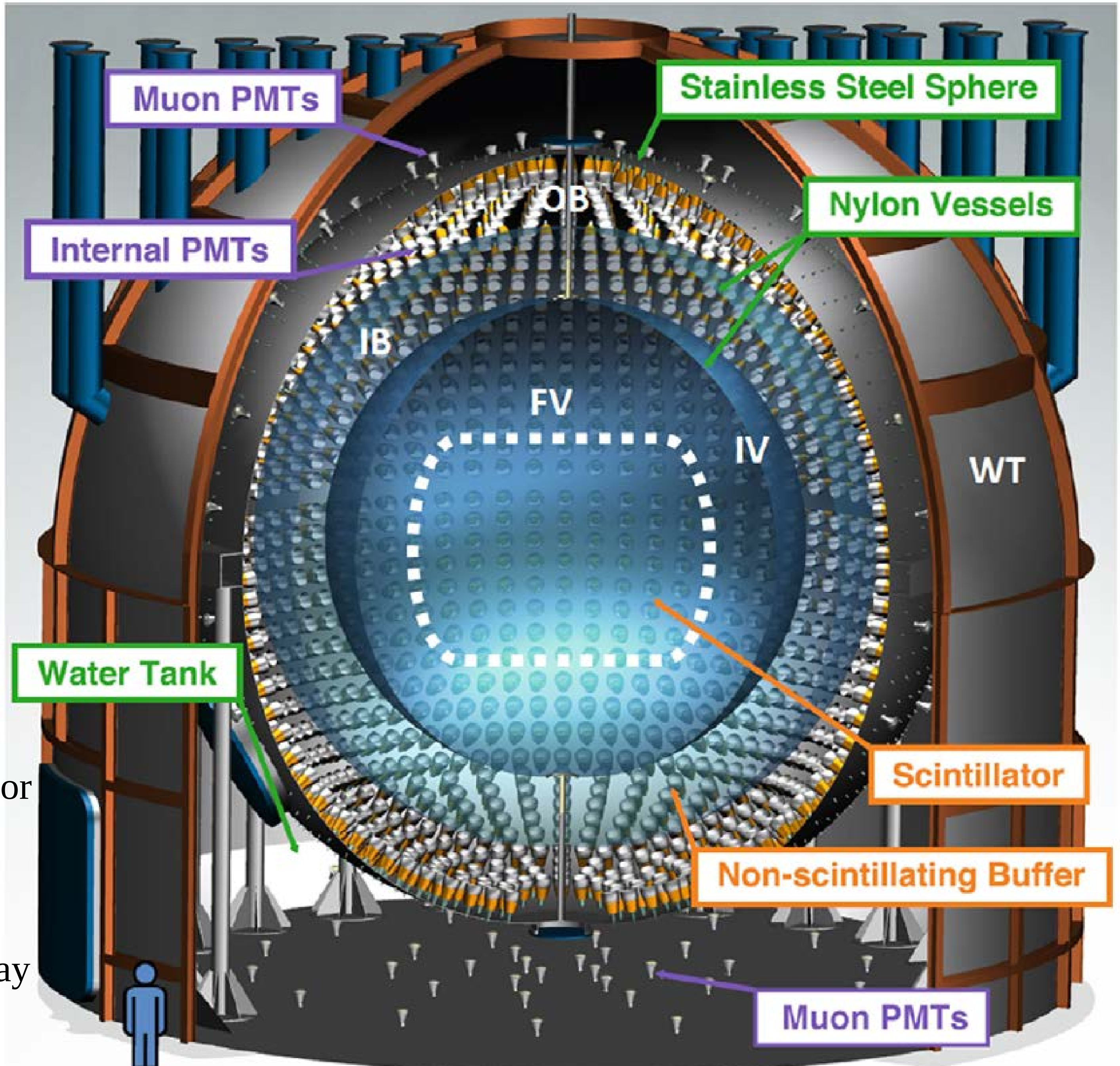

Borexino Collaboration

UNIVERSITÀ DEGLI STUDI DI MILANO

INFN Istituto Nazionale di Fisica Nucleare

LNGS

PRINCETON UNIVERSITY

UNIVERSITÀ DEGLI STUDI DI GENOVA

NATIONAL RESEARCH CENTER "KURCHATOV INSTITUTE"

St. Petersburg Nuclear Physics Inst.

Technische Universität München

JAGIELLONIAN UNIVERSITY IN KRAKÓW

JÜLICH FORSCHUNGSZENTRUM

Virginia Tech

JOHANNES GUTENBERG UNIVERSITÄT MAINZ

SKOBELTSYN INSTITUTE OF NUCLEAR PHYSICS LOMONOSOV MOSCOW STATE UNIVERSITY

Joint Institute for Nuclear Research

TECHNISCHE UNIVERSITÄT DRESDEN

RWTH AACHEN UNIVERSITY

Standard Solar Model : "engine" of the Sun, solar neutrinos production and spectrum predictions

Developed by **John Bahcall** for more than 40 years

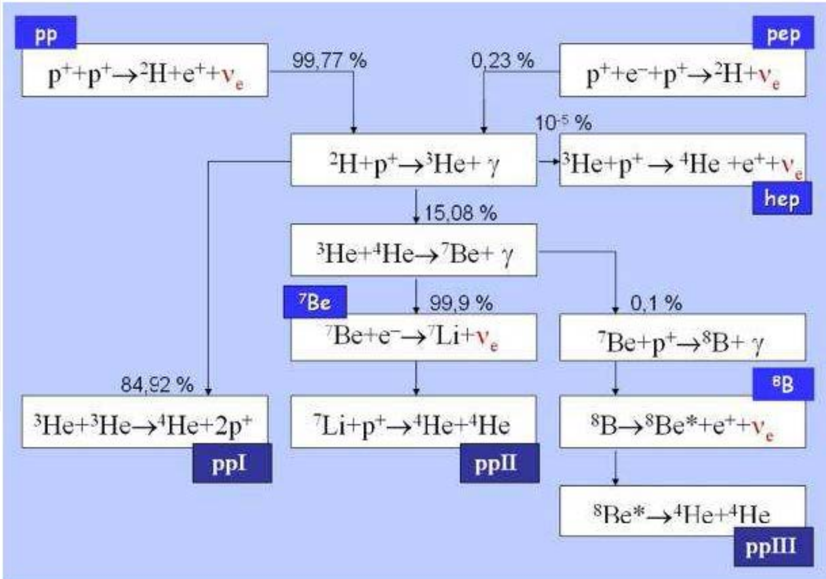

pp chain

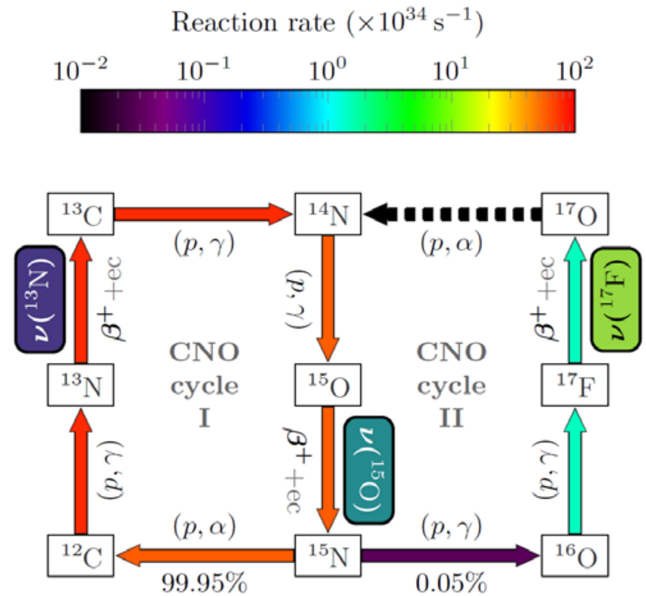

Dominant in massive stars

>99% of the energy in the Sun

the remaining <1% in the Sun ?

Latest SSM spectral prediction
A. Serenelli
EPJA, volume 5, id 78 (2016)
N. Vinyoles et al.
The Astrophysical Journal, 835:202 (16pp), 2017

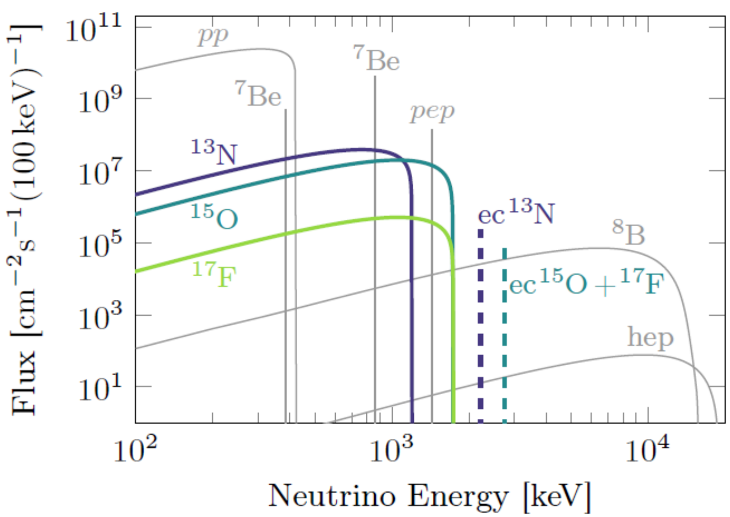

Controversy about the surface metallicity composition of the Sun: predictions differ up to 28% for the CNO ν flux using lower (LZ) or higher Z (HZ) models

The pp chain investigation as basis of the quest for CNO neutrinos

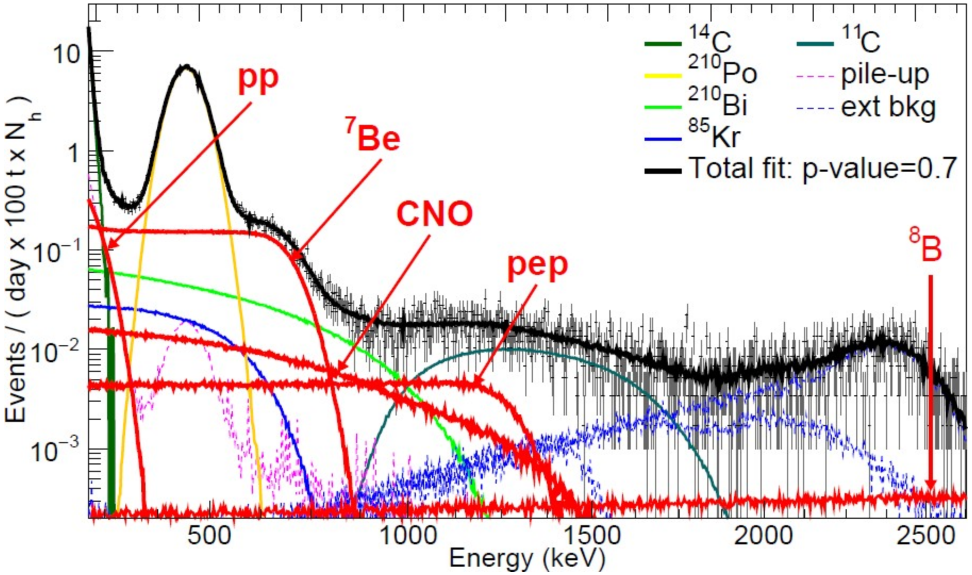

Latest pp chain published Borexino Solar neutrino spectroscopy: simultaneous fit of all the low energy neutrino solar rates

pp, ^{7}Be, pep, 8B and upper limit on hep

+ **upper limit for CNO**

→ multivariate Monte Carlo fit

But not yet an evidence and a measure

Why a CNO ν measurement is so difficult?

1) Low rate
2) No distinguishable spectral features
3) Correlation with ^{210}Bi and pep ν's

} shape

Nature, Volume 562, pp. 505-510 (2018)
Nature, Volume 512, Issue 7515, pp. 383-386 (2014)
Physical Review D, Volume 100, Issue 8, id.082004 (2019)
PHYSICAL REVIEW D 101, 062001 (2020)

} "Summa" of the Borexino pp results

The Borexino quest for CNO neutrinos after the complete pp chain measurement

CNO ν – pep ν – ^{210}Bi correlations

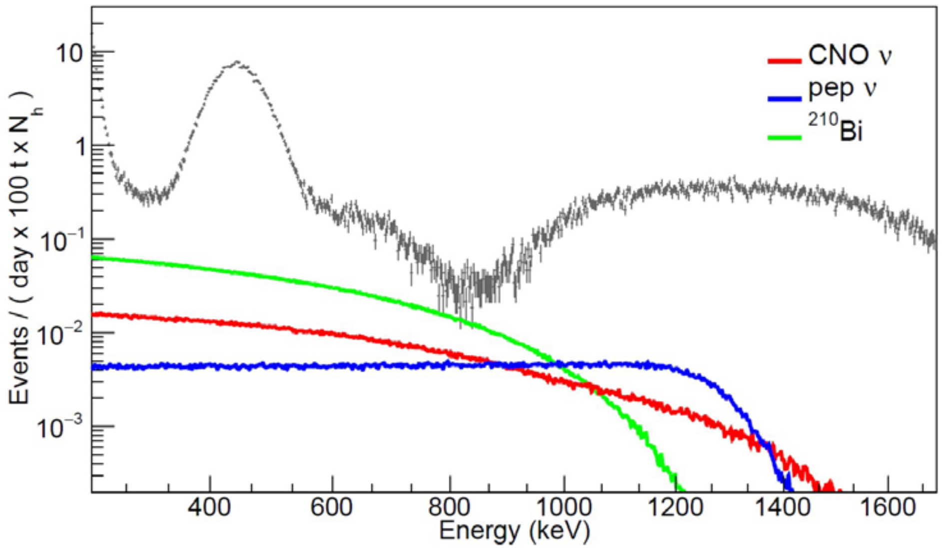

- Borexino data
- CNO ν expected spectrum
- ^{210}Bi spectrum
- pep ν spectrum

The **spectral fit** returns only the sum of **CNO** and **^{210}Bi**, if both are left free

Note also the low rates:

- R(CNO ν)$_{expected}$ ~ 3-5 cpd/100ton
- R(^{210}Bi) ~ 10 cpd/100ton
- R(pep) ~ 2.5 cpd/100ton

Thanks to Borexino unprecedented purity @ 95% C.L ^{232}Th< 5.7 10^{-19} g/g ^{238}U < 9.4 10^{-20} g/g other backgrounds less relevant apart the cosmogenic ^{11}C

The pep flux can be constrained at the 1.4 % level through the solar luminosity constraint coupled to SSM predictions on the pp to pep rate ratio and the most recent oscillation parameters - J. Bergström et al., JHEP, 2016:132, 2016

^{210}Bi independent determination from ^{210}Po

Degeneracy in the fit removable with a constraint on ^{210}Bi

Independent estimation of ^{210}Bi rate

^{210}Bi-^{210}Po analysis:
Extract the ^{210}Bi decay rate in Borexino through the study of the ^{210}Po decay rate

$$^{210}\mathrm{Pb} \xrightarrow[32\ \mathrm{y}]{\beta^-} {}^{210}\mathrm{Bi} \xrightarrow[7.23\ \mathrm{d}]{\beta^-} {}^{210}\mathrm{Po} \xrightarrow[199.1\ \mathrm{d}]{\alpha} {}^{206}\mathrm{Pb}$$

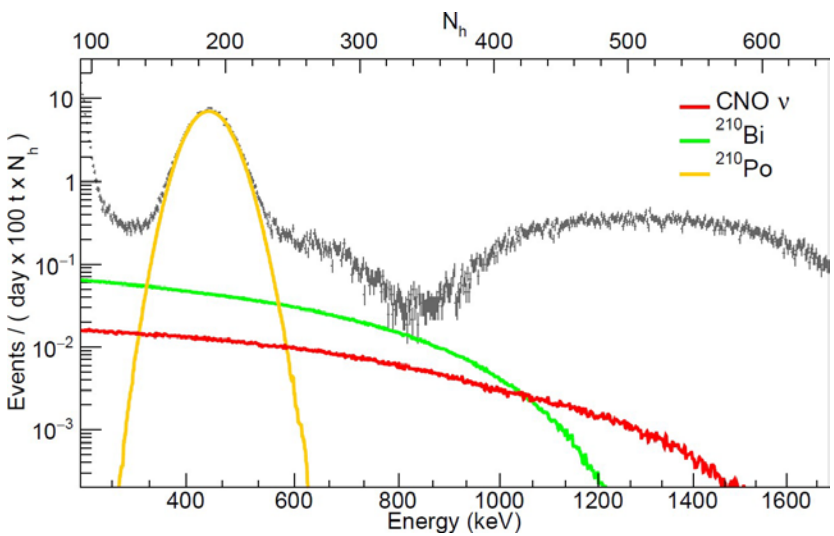

^{210}Po is "easier" to identify wrt ^{210}Bi:

- Monoenergetic decay → "gaussian" peak
- α decay → pulse shape discrimination

If the ^{210}Bi is in equilibrium with ^{210}Po, an independent measurement of the latter decay rate gives directly the ^{210}Bi one (secular equilibrium scenario)

→ The quest for CNO is turned into the quest of ^{210}Bi through ^{210}Po !

Hurdle - diffusion and convection of ^{210}Po from the vessel surface

^{210}Po moves from the vessel surface into the scintillator and within the scintillator itself $\rightarrow$ getting moved by diffusion and temperature induced convection

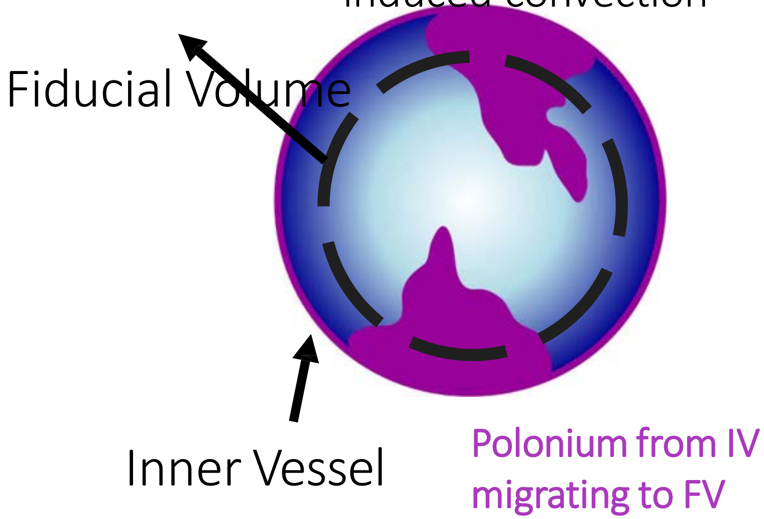

Pure exponential decay ($t_{1/2}$ =138.4 days) to the intrinsic value is perturbed by the presence of strong convective motions (purple blobs), caused mostly the seasonal and man-made temperature change in the experimental Hall

$$\partial_t \rho(r) = D\nabla^2 \rho(r) - \frac{\rho(r)}{\tau_{\mathrm{Po}}} \Longrightarrow \rho(r) = \rho_0 \frac{\sinh(r/\lambda)}{r/\lambda}$$

Diffusion length in PC

$$\lambda = \sqrt{D\,\tau_{Po}} \approx 20 \text{ cm}$$

Even tiny amount of ^{210}Pb – source of ^{210}Po - present on vessel surface are relevant at the Borexino extreme radiopurity level

without taking compensating measures convection is dominant

Example of the external temperature impact on the ^{210}Po in the scintillator

From this event the implementations from 2014 insulation layer around the tank

- active control system

→ stable north south gradient to stratify the scintillator and stop the liquid motion

And later on in 2019

- Hall C stabilization

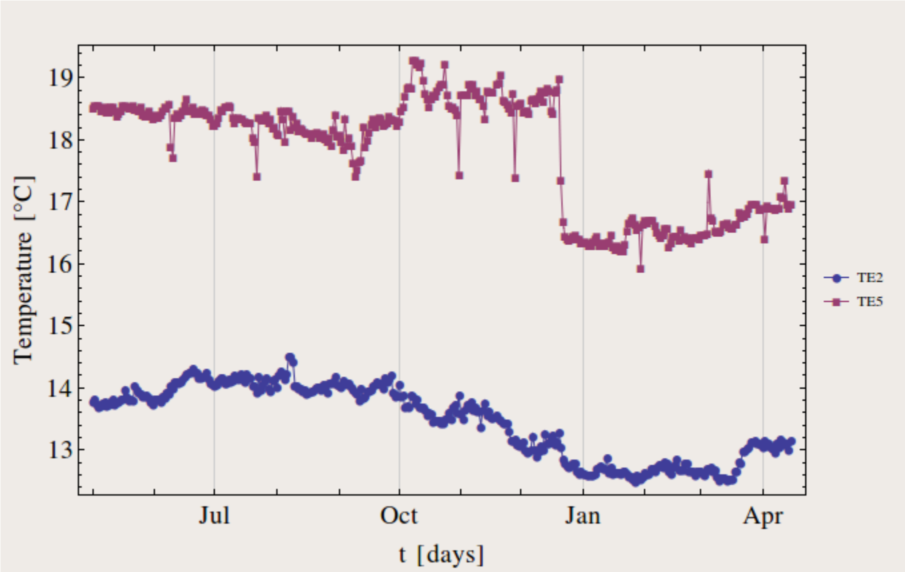

Temperature probes
TE2: 3 m from ground
TE5: on top of the Water Tank

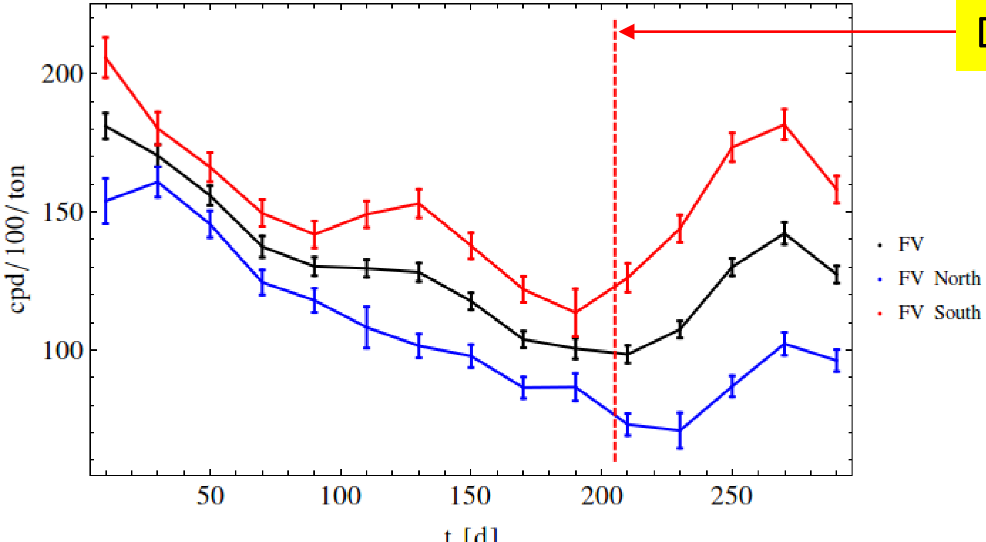

December 16th 2013

Striking effect of the temperature discontinuity on the ^{210}Po evolution

^{210}Po count rate evolution vs. time in the Fiducial Volume

Multiple approaches to monitor, understand, and suppress the temperature variations

Thermal insulation & Active Gradient Stabilization System

Temperature monitoring probes

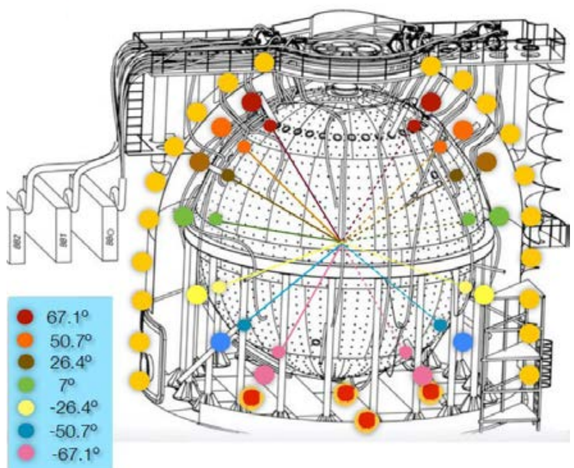

54 temperature probes

Fluid dynamical simulation

Very good agreement with measured temperatures

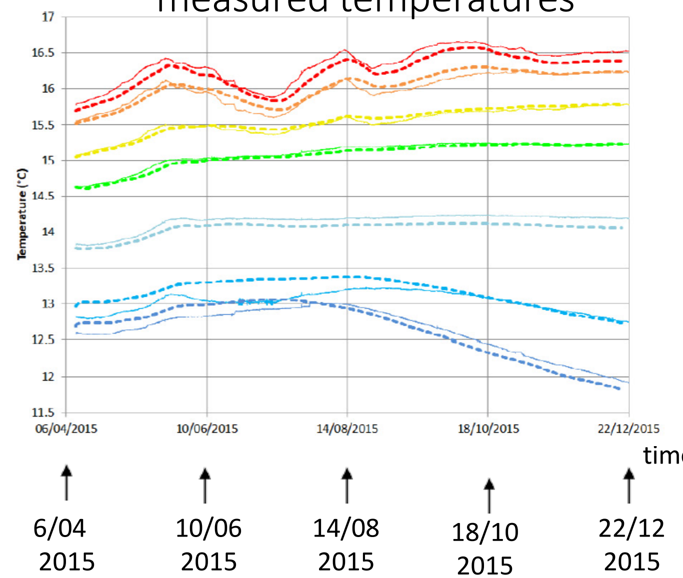

- Double layer of mineral wool (thermal conductivity down to 0.03 W/m/K) & Active Gradient Stabilization System (2014-2016)
- Temperature Probes (2014-2015)
- Fluid dynamical simulations
- Hall C Temperature Stabilization (2019)

V. di Marcello et al., NIM A 964, id. 163801

Enduring effort over the past six years

Insulation of the Water Tank

- The Water Tank covered starting from the floor, all around the circumference, up to the total height including the organ pipes
- The thickness of the insulation double layer is 200mm
- The first layer in contact with the tank is a naked roll of rock wool
- The second layer of insulation is a roll with reinforced grid and aluminum outside
- The total insulation layer kept in place using proper pins glued to the Water Tank wall using a low rad glue
- 7-8 pins installed for square meter of insulation

The upper part of installation accomplished using proper scaffolding

Instrumentation of the detector for thermal stabilization and monitoring

Borexino Water Tank after the completion of the thermal insulation layer

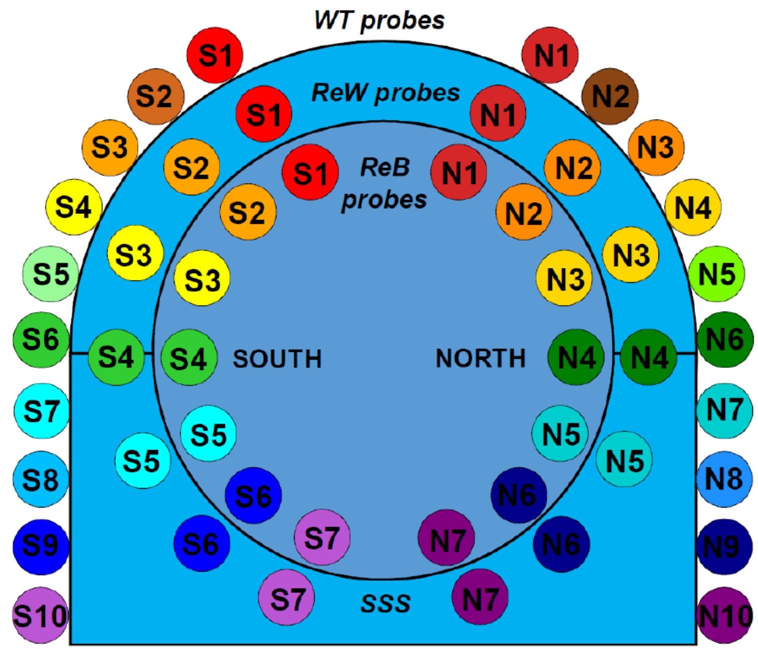

Distribution of temperature probes around and inside the Borexino detector

Top-Bottom gradient and active temperature control system

Controlled temperature water flowing in copper serpentines

6th band: copper coils under insulation;

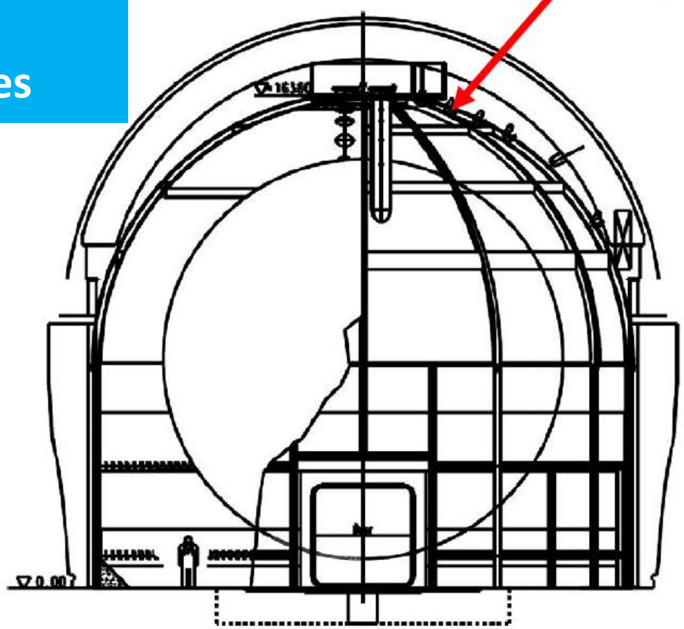

Key to ensuring a static liquid condition was the establishment of a stable top-bottom temperature gradient

The bottom temperature was established by the rock temperature

The water in the serpentines controls the top temperature $\rightarrow$ top-bottom gradient stabilized

Temperature Active Control System setup

- ✓ # 12, ~ 18 m long, ϕ = 14 mm copper coils;
- ✓ Multilayered pipe for tranfer line;
- ✓ Manifold with 12 input/output;
- ✓ Circulation pump (3 m^3/h);
- X Heater (3 kW);
- X # 6 temperature probes for wt temp monitor;
- X # 6 temperature probes for water outlet temp monitor;
- X Temperature controller;
- X Massflowmeter.
- X Slow Control software

Hall C temperature control system

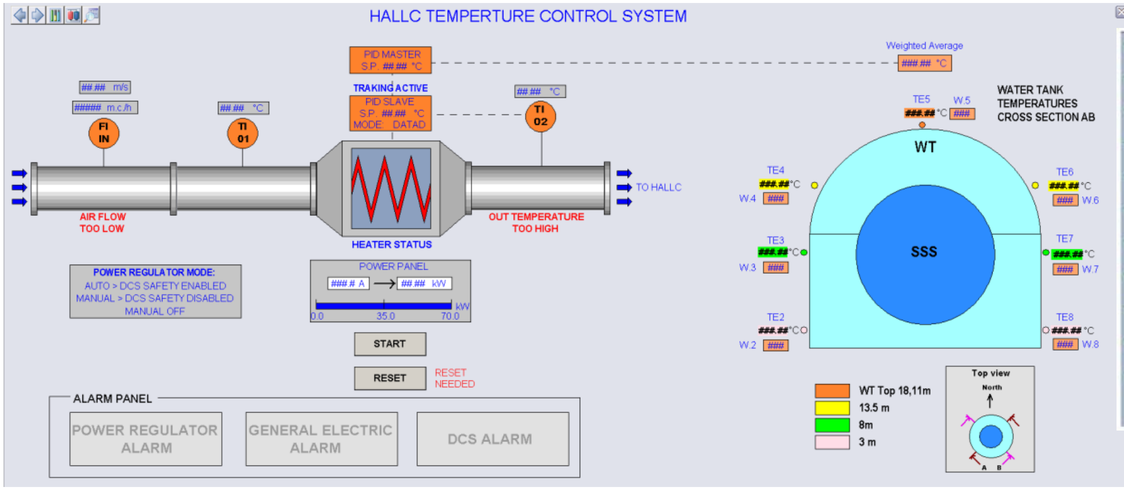

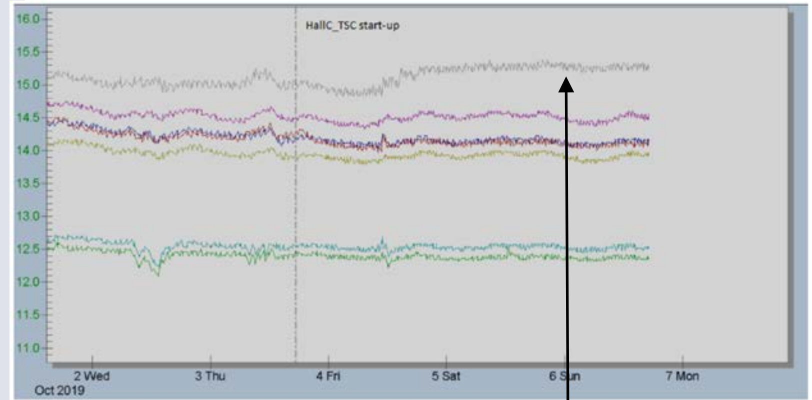

Early effect

It monitors and regulates the inlet air from the air duct to Hall C and can work in direct and feedback mode

- Switched on in non feedback mode beginning of October 2019
- Passed to feedback mode (feedback signals from the central external sensors of the Water Tank/Hall C) after one month

Temperature evolution from the probes

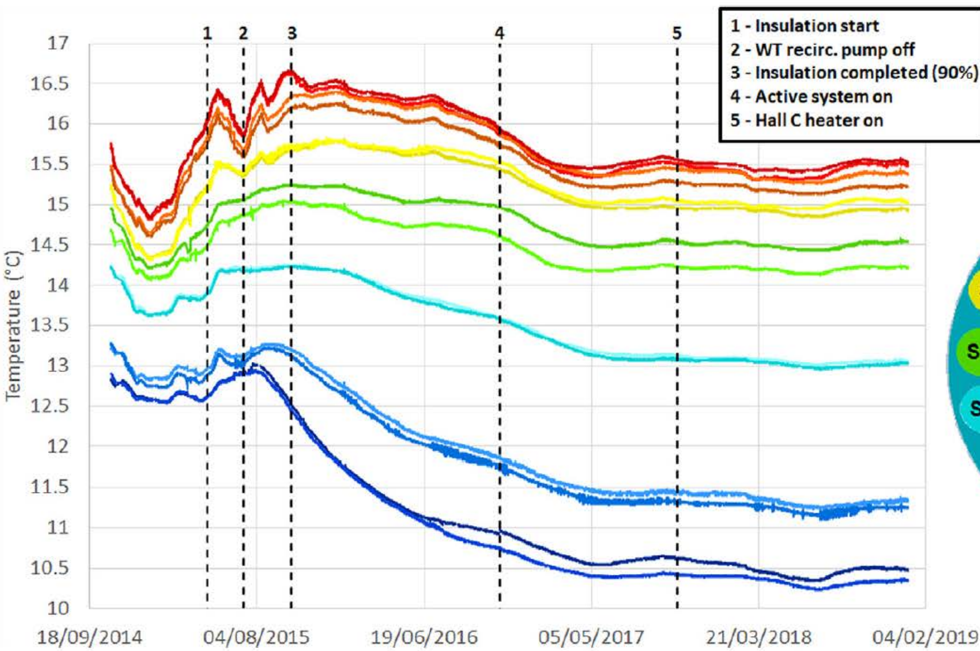

Global view of stabilization from 2015

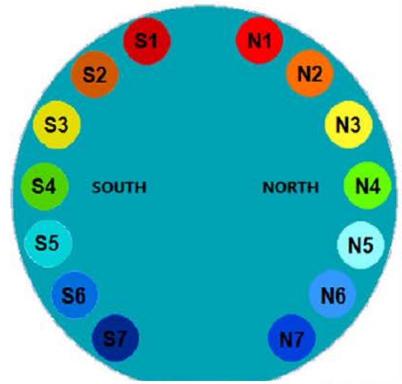

Probes sensing the outer buffer

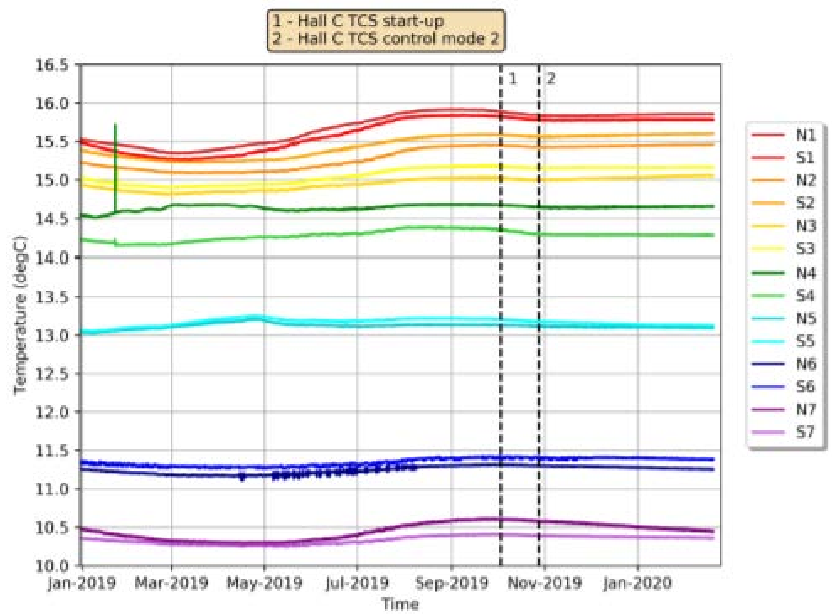

Snapshot of the last year

Achieved excellent temperature stability with the establishment of a clear temperature gradient

Probes resolution 0.07 °C

Further global view of the recent temperature evolution

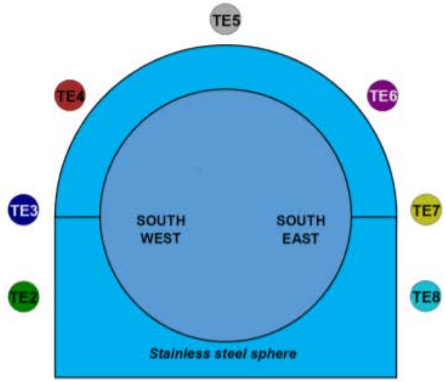

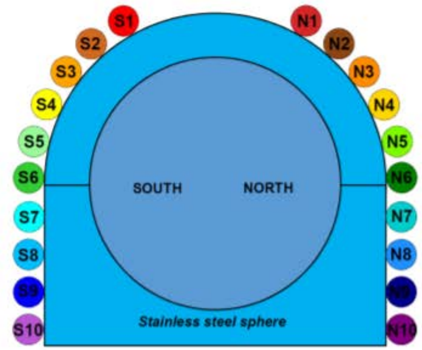

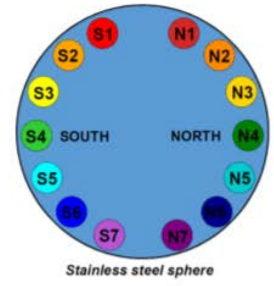

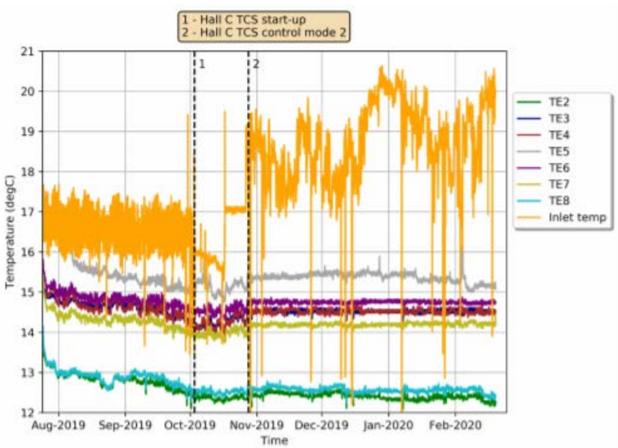

Figure 9: Air temperature profile around Borexino. The orange curve is the measured temperature of the Hall C inlet air.

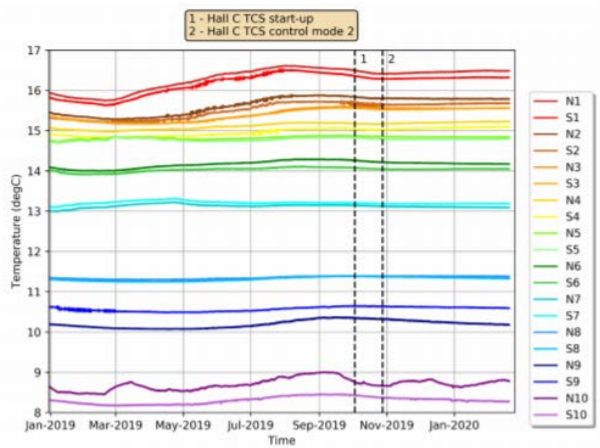

Figure 10: Water tank surface temperature evolution.

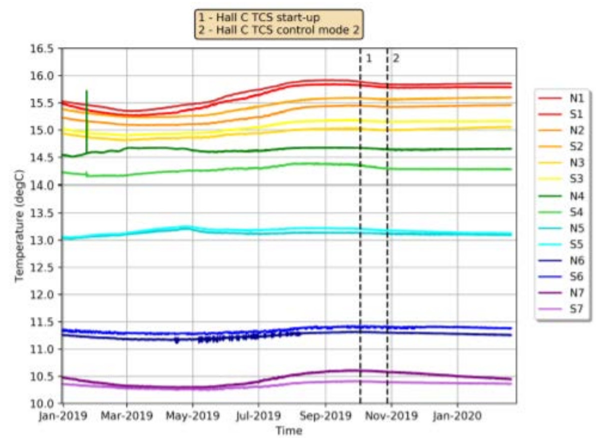

Figure 11: Re-entrant buffer temperature evolution.

Air around the Tank

On the surface of the Tank

Inside the outer buffer

From November 2019 achieved the best temperature stability ever

A 2D detailed view - Polonium data spatial mapping vs. time

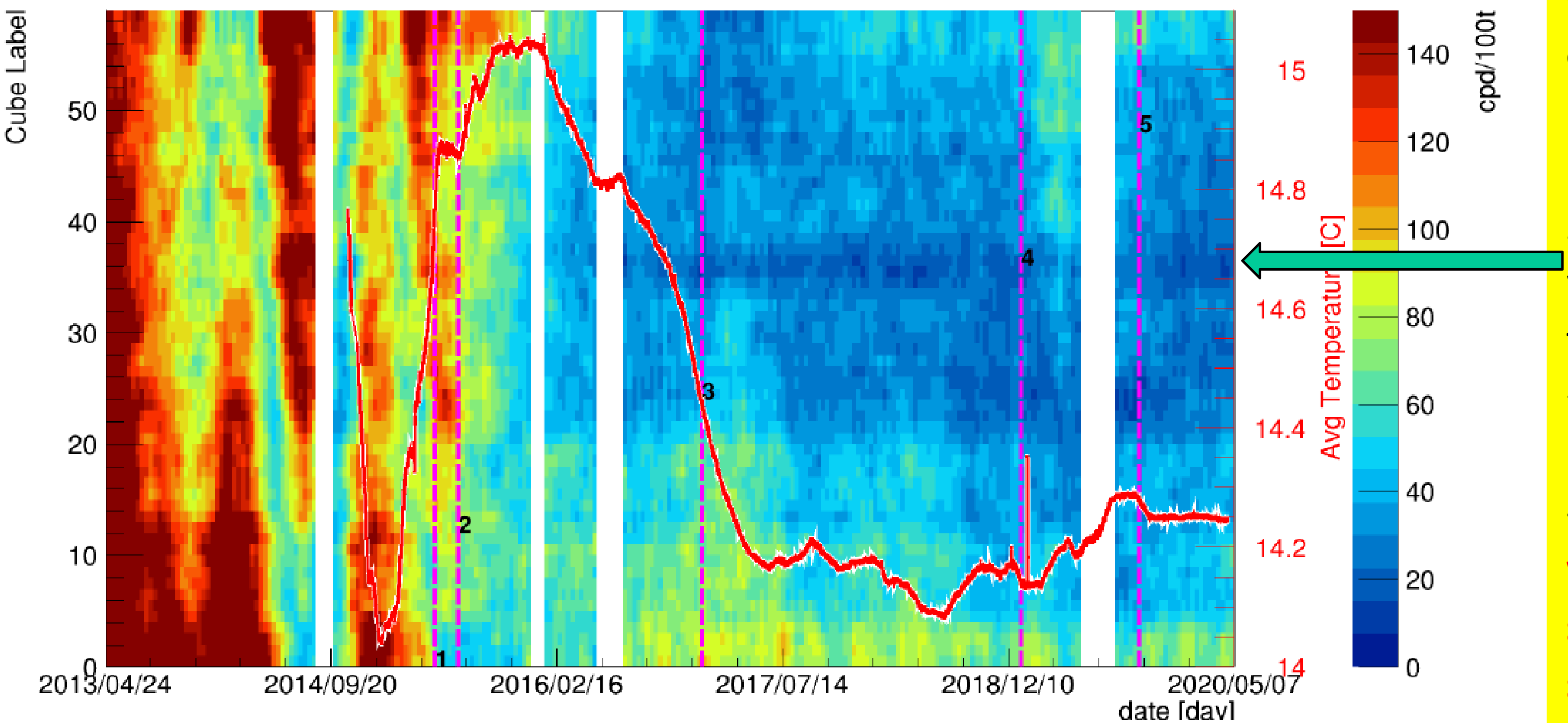

Crucial observation: "Low Polonium Field" 20 tons size from which we can infer the intrinsic ^{210}Po and hence the ^{210}Bi - **agreement with simulations see next slides**

Convective condition before insulation

Quiet situation after insulation

1. Beginning of the Insulation Program
2. Turning off the water recirculation system in the Water Tank
3. Start of the active temperature control system operations
4. Change of the active control set points
5. Installation and commissioning of the Hall C temperature control system.

Stabilization measures were very effective at reducing the ^{210}Po motion

Low Polonium Field inside the scintillator

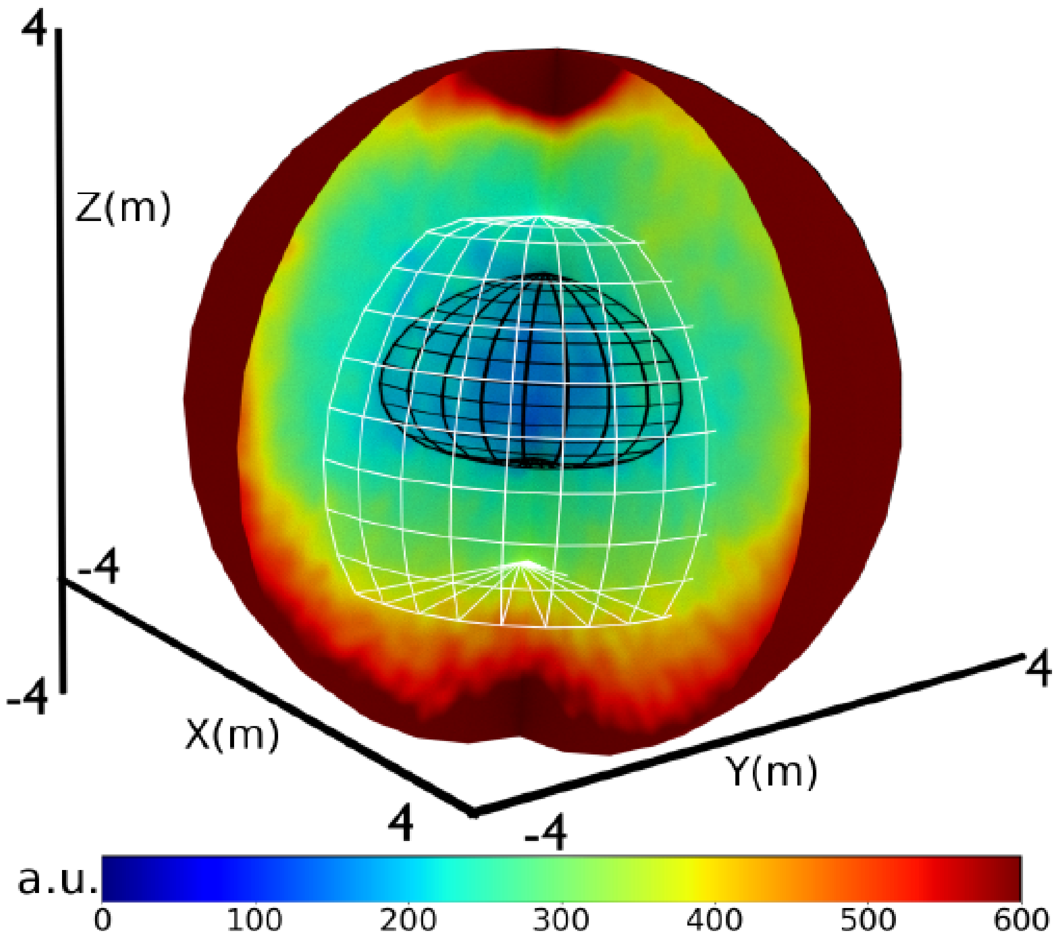

Three-dimensional view of the ^{210}Po activity inside the entire Inner Vessel - the innermost blueish region contains the LPoF (black grid) - the white grid is the software-defined Fiducial Volume

Prediction of ^{210}Po volumetric pattern – Fluid dynamical simulation with the insulation cover of the Water Tank and the measured temperature profiles

^{210}Po rate vs. time within the vessel (initial condition and final solution displayed) taking into account a surface distribution on the wall of the vessel. The simulation describes the migration due to the residual convective motion post-insulation

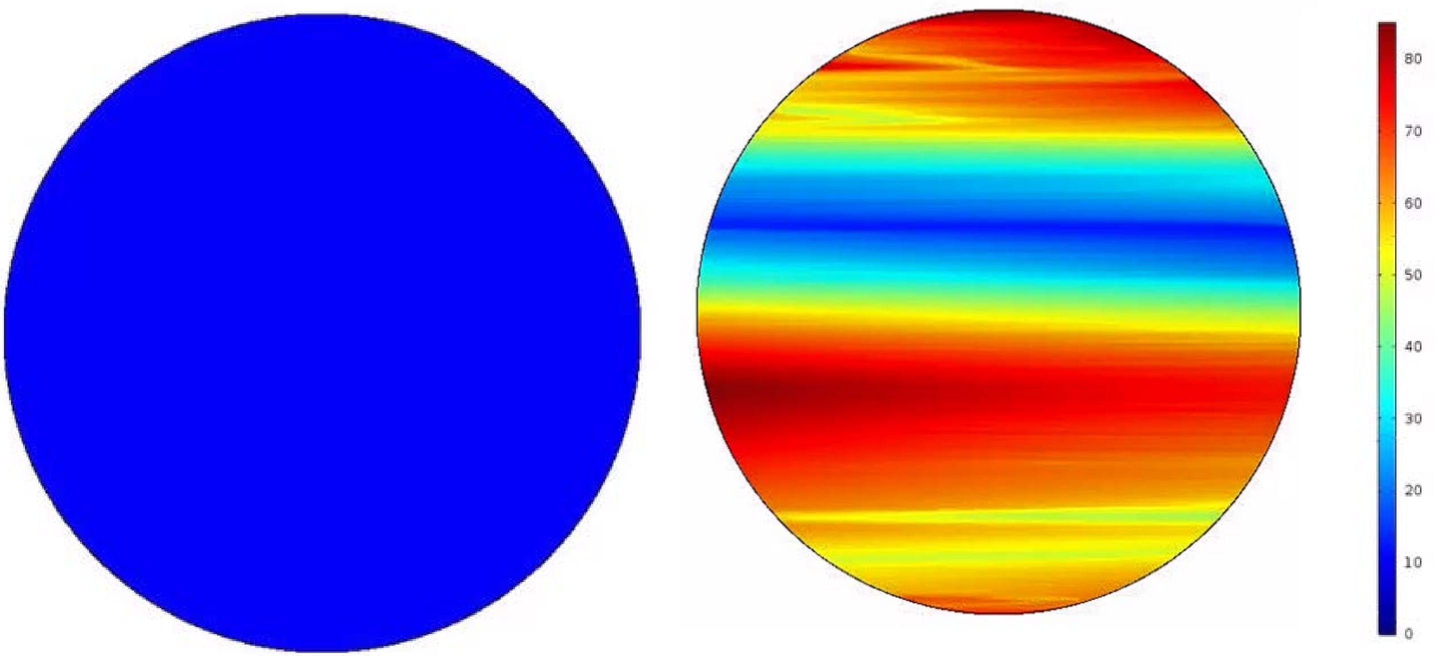

Initial uniform

End of the simulated period

Predicted more residual "turbulence " (and hence Polonium) in the bottom and the dynamical formation of a "minimum" ^{210}Po region above the equator, unaffected by the ^{210}Po influx from the surface

^{210}Bi upper limit from ^{210}Po data

- ^{210}Po (alpha) events are fitted to find the minimum ^{210}Po rate in the sub-region
- Low Polonium Field (LPoF) at around 80cm above equator, but it moves over time very slowly
- “Aligning” the data:
  1. Fit paraboloid/spline over monthly data
  2. Extract z-position (z0) over time
  3. Create “aligned” dataset where each data point is shifted with the z0 from the previous month. This reduces bias in the final result.

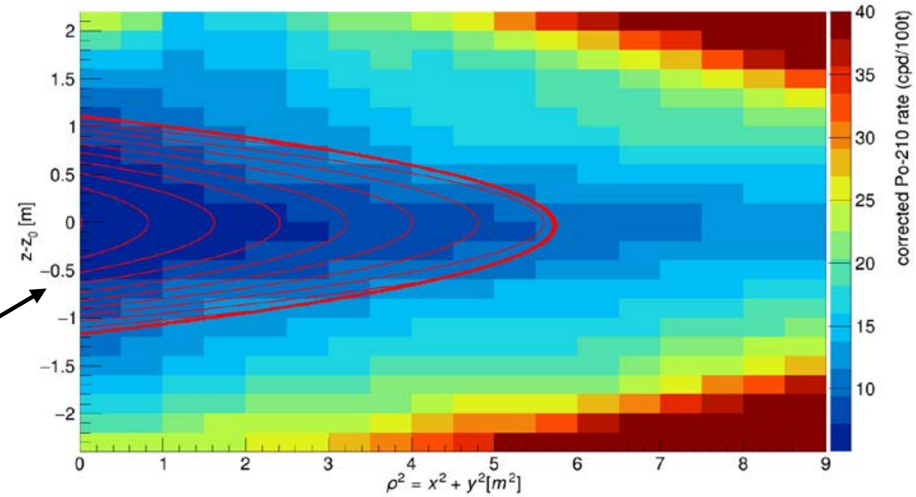

Distribution of ^{210}Po events in the blindly aligned data-set

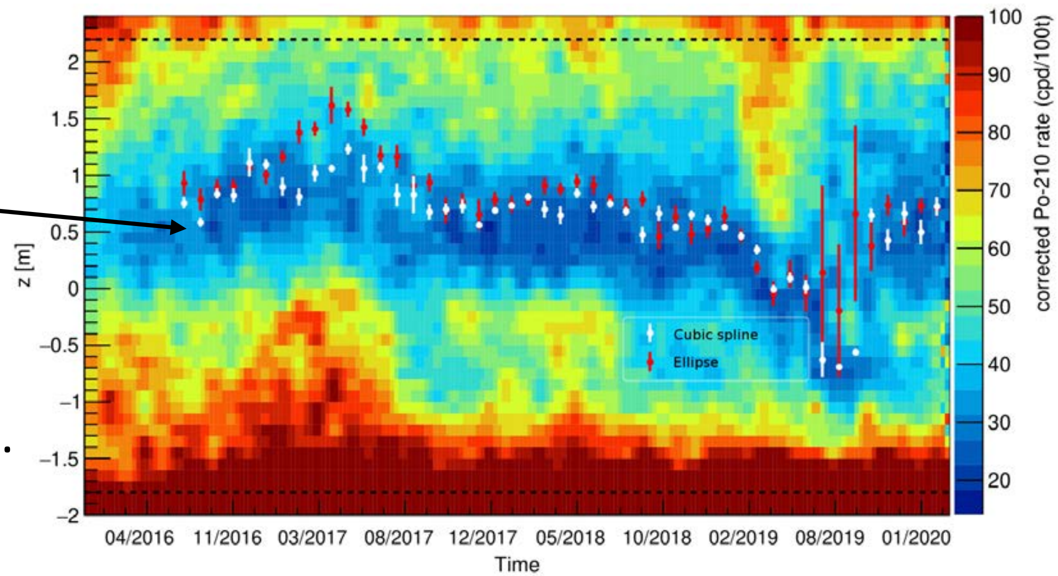

Reconstructed central position of LPoF over time for different methods

Fitting the aligned ^{210}Po data

Paraboloid

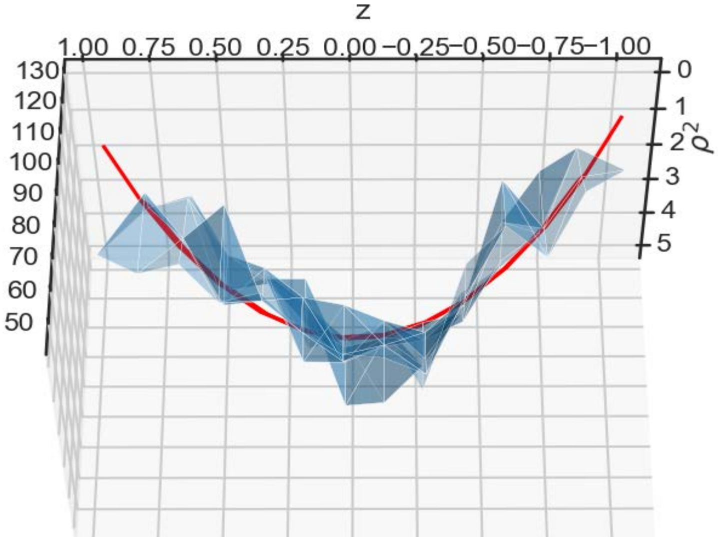

$$R_{Po} = R_{min}\epsilon \cdot \left(1 + \frac{\rho^2}{a^2} + \frac{(z - z_0)^2}{b^2}\right) + R_\beta$$

Spline fit:

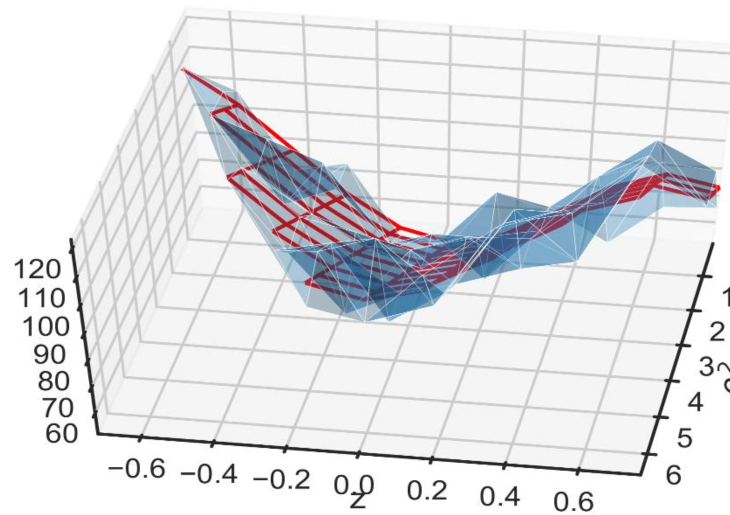

Account for complexity along the z axis with a cubic spline model using a Bayesian nested sampling algorithm

Both methods agree within systematics:

$R_{min}(cpd/100t)$	σ_{fit}	σ_{mass}	$\sigma_{binning}$	σ ^{210}Bi homog.	$\sigma_{\beta\ leak}$	σ_{Total}
11.5	0.88	0.36	0.31	See next slides	0.30	See next slides

^{210}Bi spatial uniformity systematics

^{210}Bi constraint based on 20t region analysis

→ CNO analysis: implicitly extrapolating the ^{210}Bi constraint from the LPoF to the larger FV mass (70t)

Precision level we state ^{210}Bi uniformity in the FV?" → systematic to the ^{210}Bi spatial

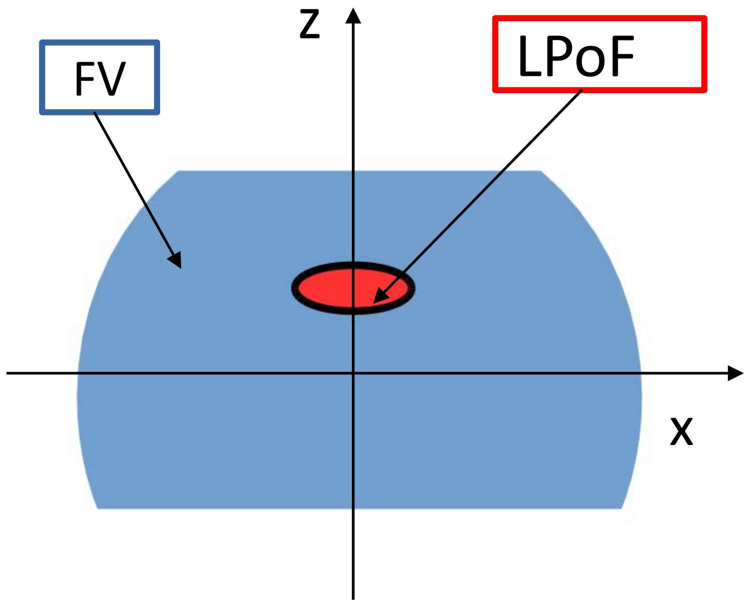

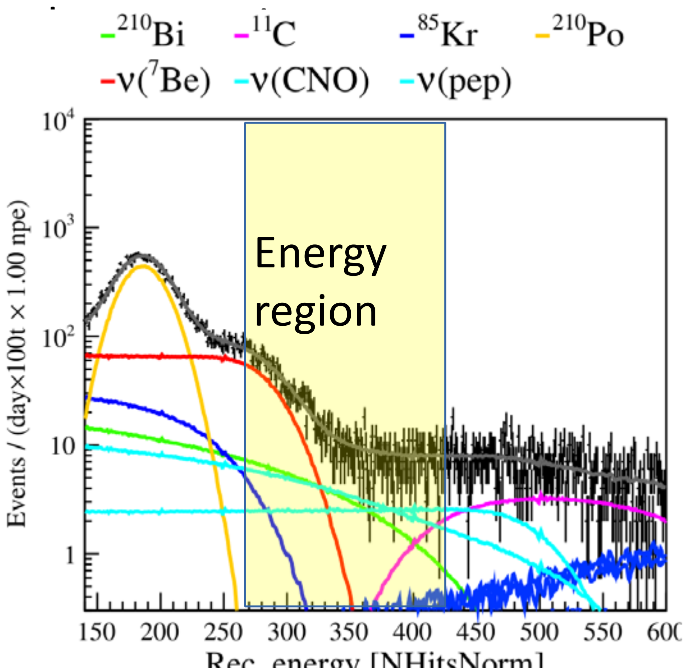

Analyzing β spatial distribution of events in a large energy range (0.554 MeV < E < 0.904 MeV)

→ ~75% neutrinos
→ ~15% ^{210}Bi
→ ~10% ^{11}C and ^{85}Kr

Rate variations are attributed to ^{210}Bi events (conservative approach)

^{210}Bi spatial uniformity systematics

Radial β analysis + **Angular β analysis**

Radial shells

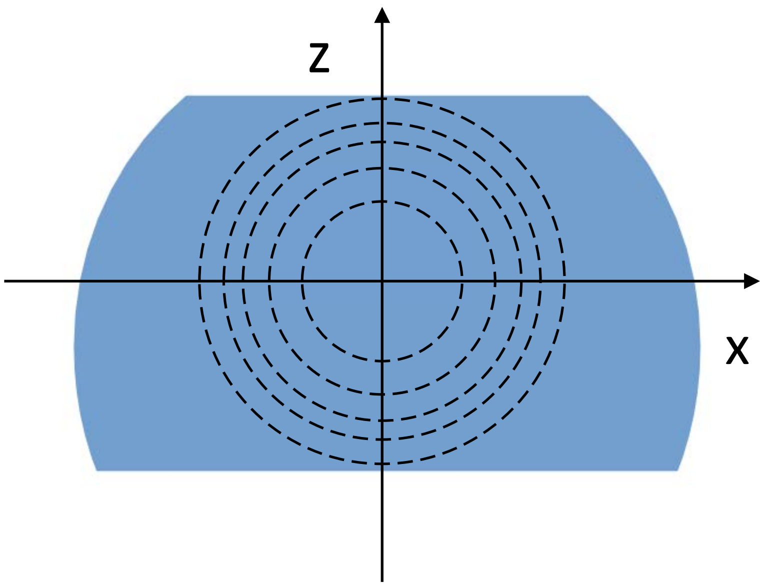

Spherical harmonics decomposition

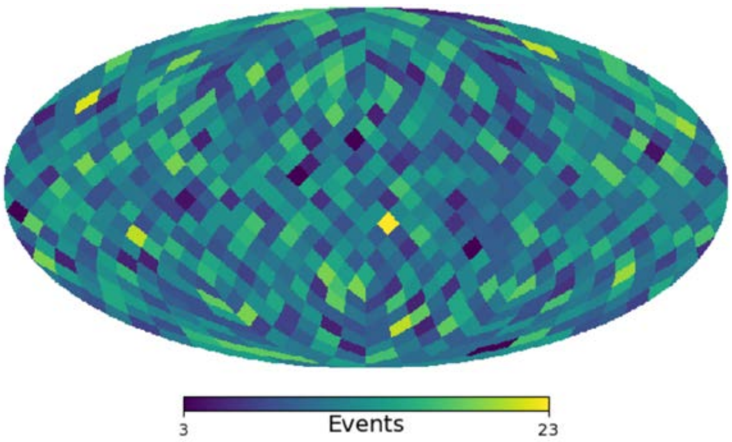

0.51 cpd/100t

0.59 cpd/100t

Overall ^{210}Bi spatial uniformity systematics: 0.78 cpd/100t

^{210}Bi spatial uniformity systematics angular and radial derivations

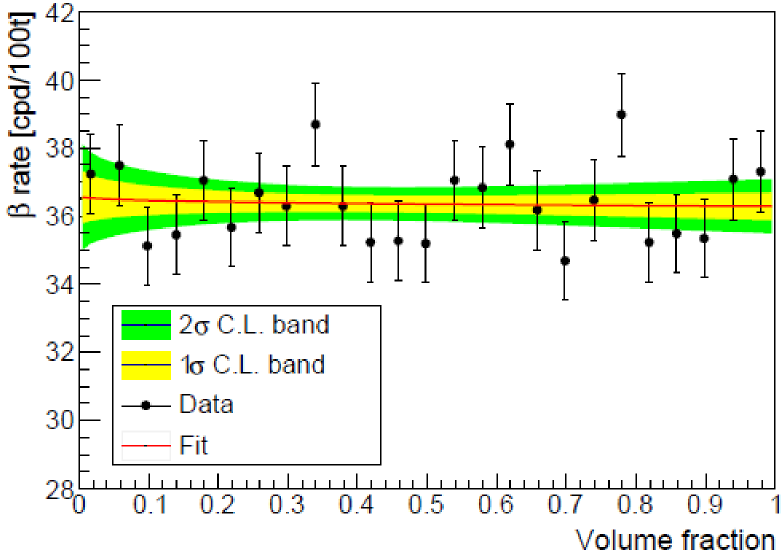

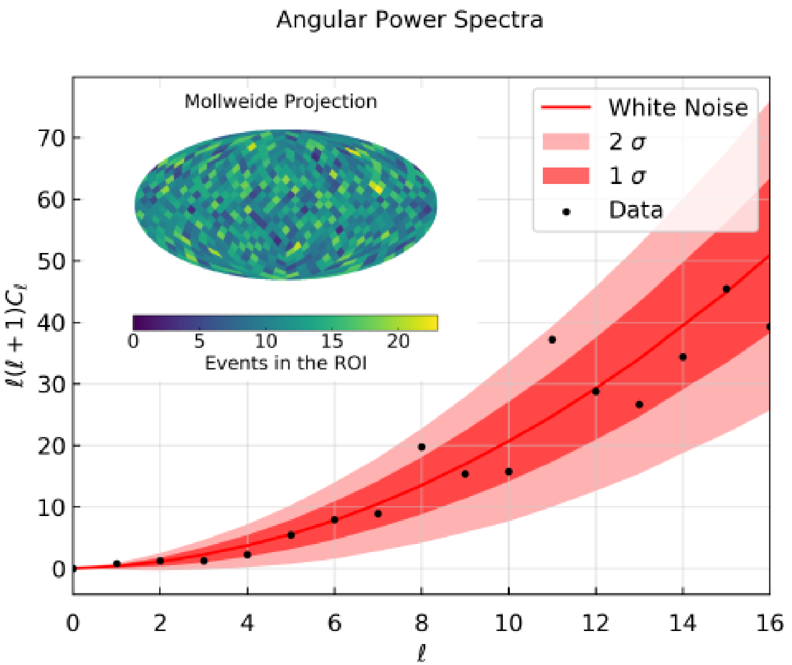

Linear fit performed over the variable r/r_0 where r_0 is the radius of the sphere surrounding the analysis fiducial volume data are found compatible with a uniform distribution within 0.51 cpd/100t

Angular spectral density of observed β events in the ^{210}Bi ROI (black points) compared with 10000 uniform event distributions from Monte Carlo simulations at one (dark pink) and two σ CL (pink)
data are found compatible with uniform distribution within the uncertainty of 0.59 cpd/100t - inset: angular distribution of the β rate in the ^{210}Bi ROI

Simulation of the ^{210}Pb/^{210}Bi uniformity

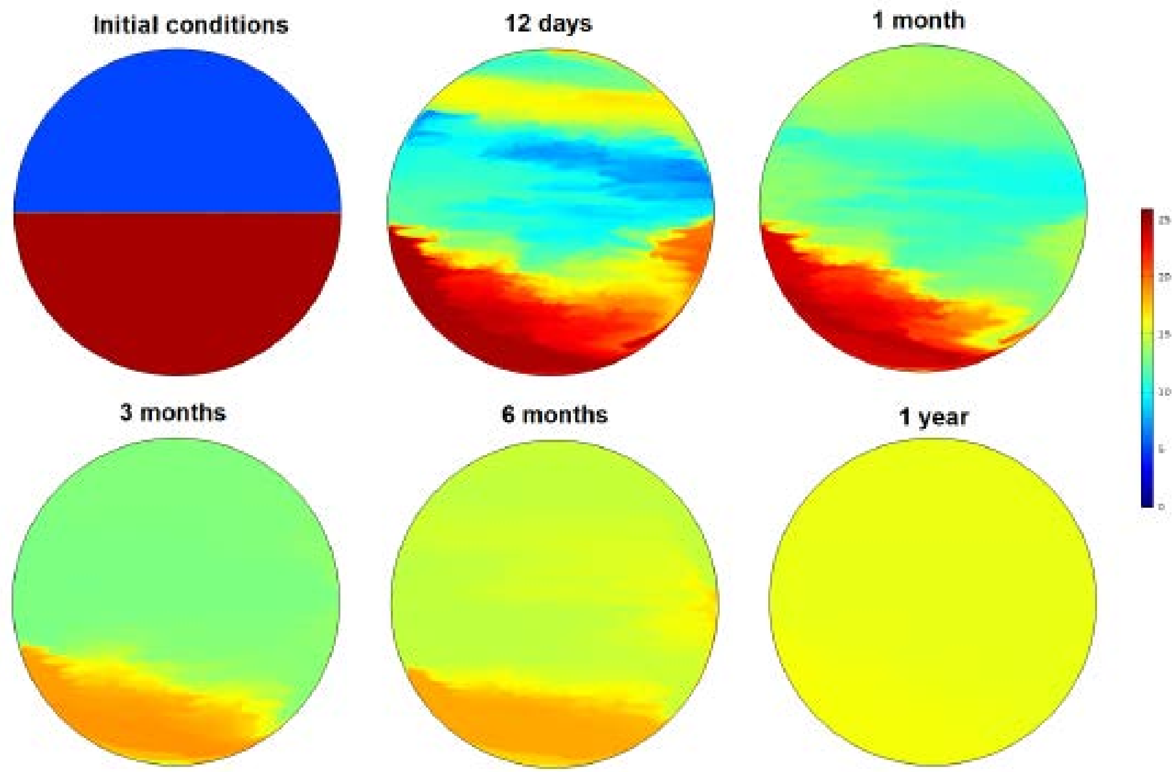

Evolution of an initial non uniform ^{210}Pb/^{210}Bi distribution pre-insulation and with the experimental temperature distributions at that time → **uniformity** reached in 1 year in the entire inner vessel

^{210}Po and ^{210}Bi final numerical assessment

$$^{210}\mathrm{Pb} \xrightarrow[(23\mathrm{y})]{\beta^-} {}^{210}\mathrm{Bi} \xrightarrow[(5\mathrm{d})]{\beta^-} {}^{210}\mathrm{Po} \xrightarrow[(138\mathrm{d})]{\alpha} {}^{206}\mathrm{Pb}\,(\mathrm{stable})$$

Basis of the approach

^{210}Po rate inferred from the Low Polonium Field with all errors

$R_{min}(cpd/100t)$	σ_{fit}	σ_{mass}	$\sigma_{binning}$	$\sigma_{^{210}Bi\ homog.}$	$\sigma_{\beta\ leak}$	σ_{Total}
11.5	0.88	0.36	0.31	0.78	0.30	1.3

The ^{210}Po evaluated rate still possibly contaminated with residual ^{210}Po from the vessel surface → upper limit to the rate of ^{210}Bi

$R(^{210}Bi) \leq 11.5 \pm 1.3$ cpd/100t

Sought constraint essential to break the degeneracy with CNO →
Outcome of the relentless years-long effort to stabilize the detector and understand the ^{210}Po behavior in the Inner Vessel

MV fit CNO-ν analysis
Three distributions in the multivariate fit

TFC-subtracted spectrum

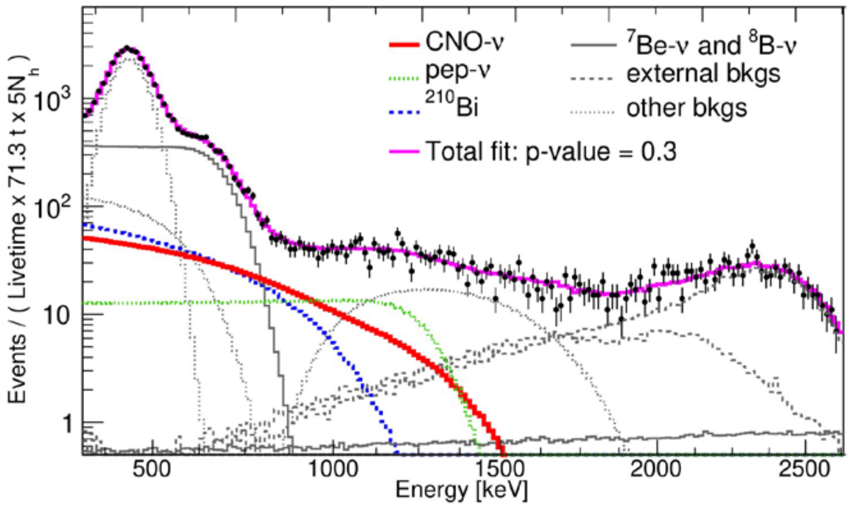

TFC-tagged spectrum

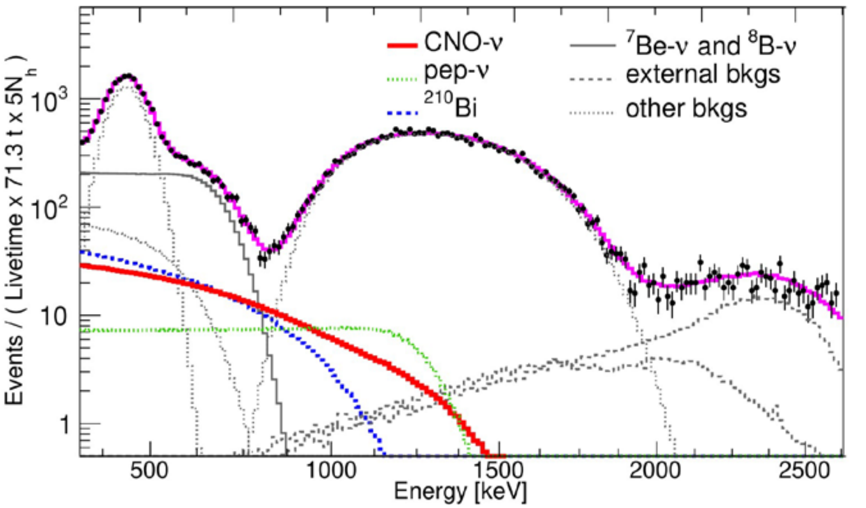

Radial distribution of events

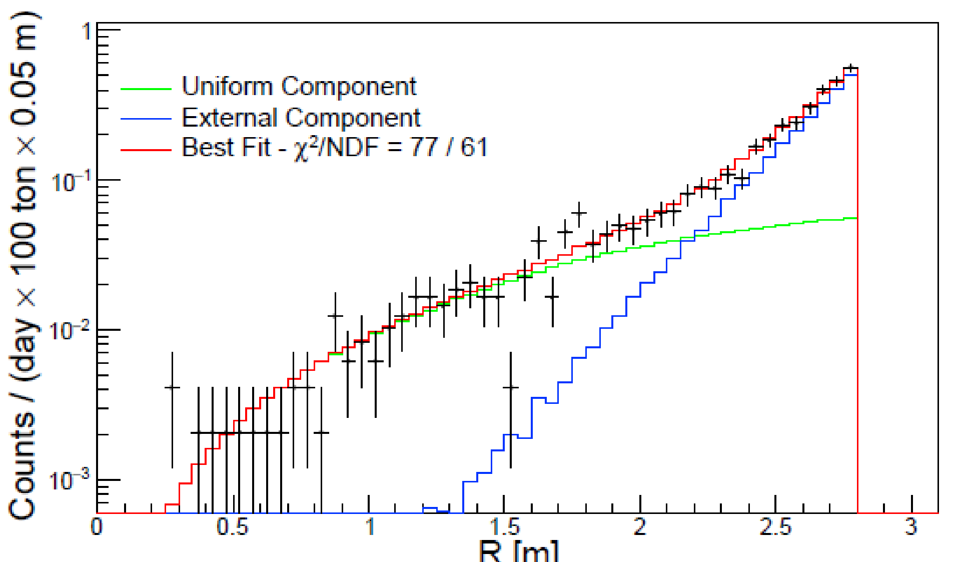

CNO-ν analysis: Phase-III MV fit

TFC-subtracted spectrum

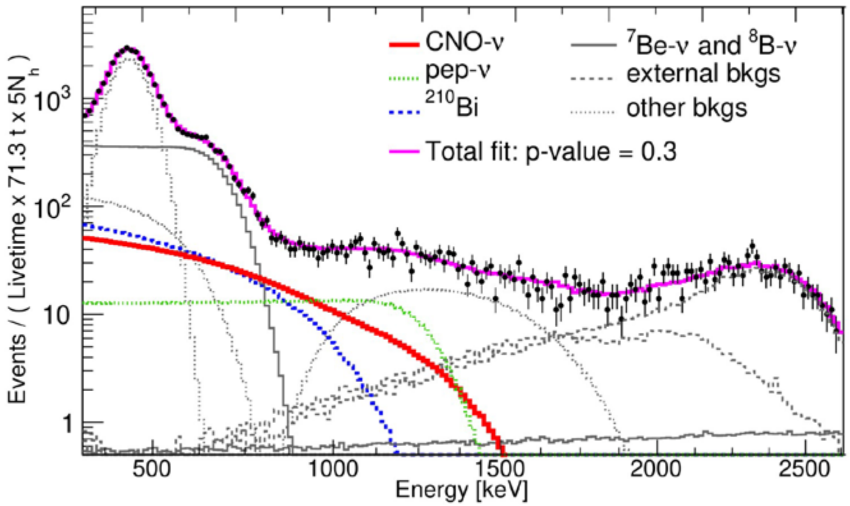

TFC-tagged spectrum

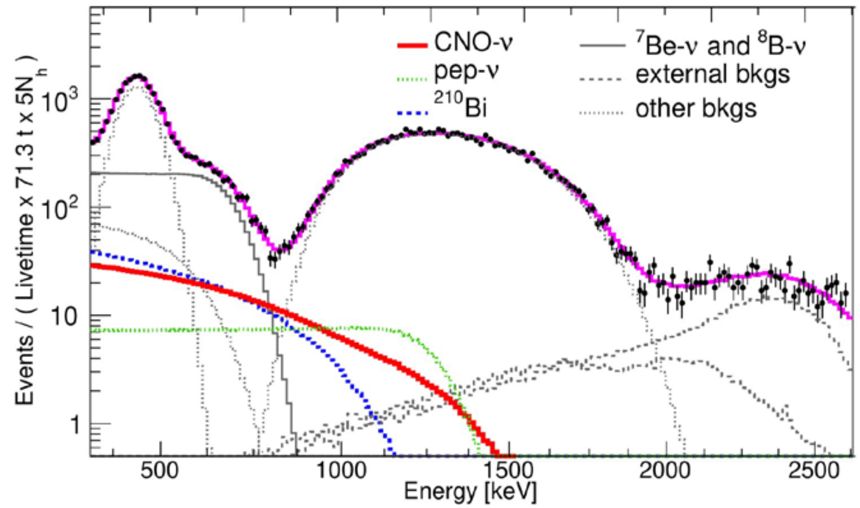

Multivariate fit (0.32-2.64 MeV)
July '16 – February '20

Maximization of a binned likelihood **3 distributions simultaneously**:

- Reconstructed energy for TFC-tagged and TFC-subtracted datasets (^{11}C identification)
- Radial position

pep-ν rate constrained → solar luminosity constraint
^{210}Bi rate constrained → **^{210}Bi-^{210}Po tagging**
CNO rate → free to vary
Other ν and bkg rates → free to vary

Result

CNO best fit 7.2 cpd/100t
asymmetric confidence interval -1.7 +2.9 cpd/100t
(stat only) asymmetry ↔ ^{210}Bi upper limit

Systematic sources and final CNO-ν result

Monte Carlo → simulate distorted datasets, fit with un-distorted PDFs

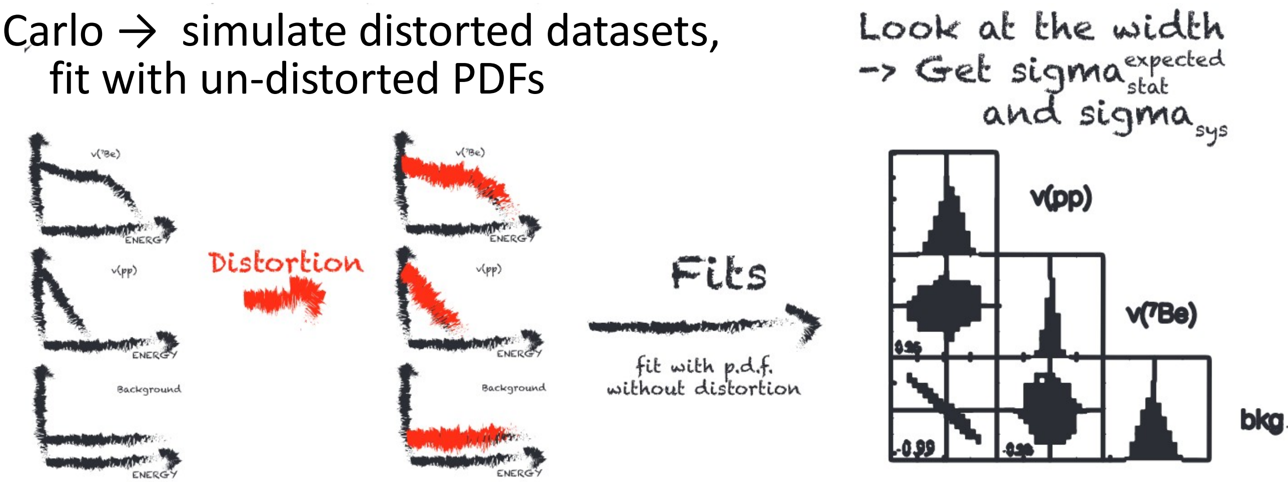

1) Fit conditions → negligible

2) ^{11}C spectrum deformation by noise cuts

3) Energy response function: energy scale (~0.23%), non-uniformity (~0.28%), non-linearity (~0.4%) from detector calibration

4) ^{210}Bi spectral shape (diff.~18%)

Final syst:
-0.5 +0.6 cpd/100t

⇒ Final CNO result 7.2 (-1.7 +3.0) cpd/100t stat + sys

corresponding to a flux of neutrinos on Earth of $7.0\ (-1.9\ \ +2.9)\times10^{8}\ cm^{-2}\ s^{-1}$

Significance of CNO-ν detection

Likelihood ratio test

Determination of the q_0 discovery test statistic from the likelihood with and without the CNO signal

G. Cowan et al., Eur. Phys. J. C, 71:1554,2011

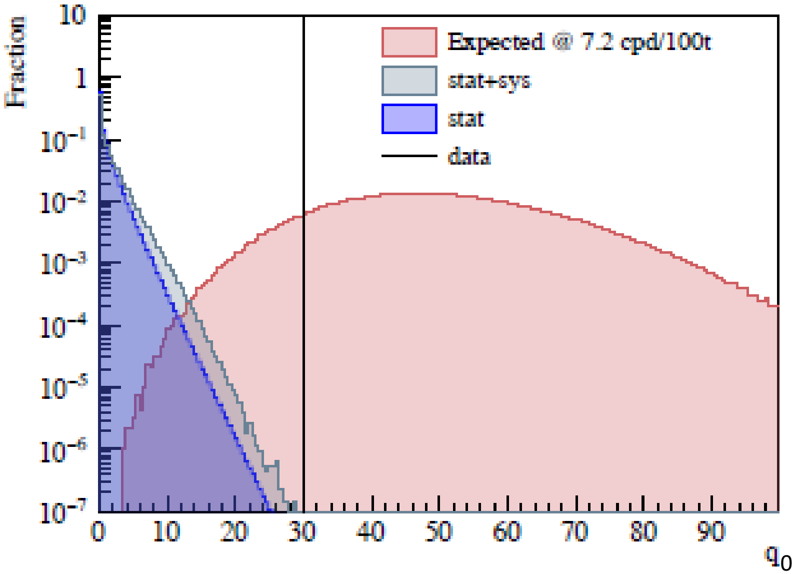

13.8 millions pseudo-datasets with deformed PDFs and no CNO to determine the q_0 reference distribution

q_0(data) from the real dataset

From the MC distributions **p-value** of q_0 (grey curve) with respect to q_0 (data) (black line) → correspondingly **significance** greater than **5 σ** at 99% CL
Consistent with **5.1σ** through the log-likelihood from the fit folded with uncertainties

No CNO hypothesis disfavored at 5 σ

With these results Borexino marks the first detection ever of CNO solar neutrinos

Result corroborated by a simplified Counting Analysis

We perform a counting analysis in a Region of Interest (ROI) determined maximizing a S/B Figure of Merit and using an analytical modeling of the detector response.

Species (S_i)	Events	Fraction
N	823 ± 28.7	
^{210}Bi	261.5 ± 29.6	0.31
ν(pep)	171.7 ± 2.4	0.21
$\nu(^7$Be)	86.8 ± 2.6	0.10
^{11}C	57.9 ± 5.8	0.07
Others	15.6 ± 1.6	0.02
$\sum_i S_i$	593.5 ± 30.4	0.71
$N - \sum_i S_i$	229.5 ± 41.8	0.29

Number of expected events of ^{210}Bi and pep neutrinos in the ROI is calculated according to the same bounds used in the MV fit

For the other species we use a reference response model of the detector

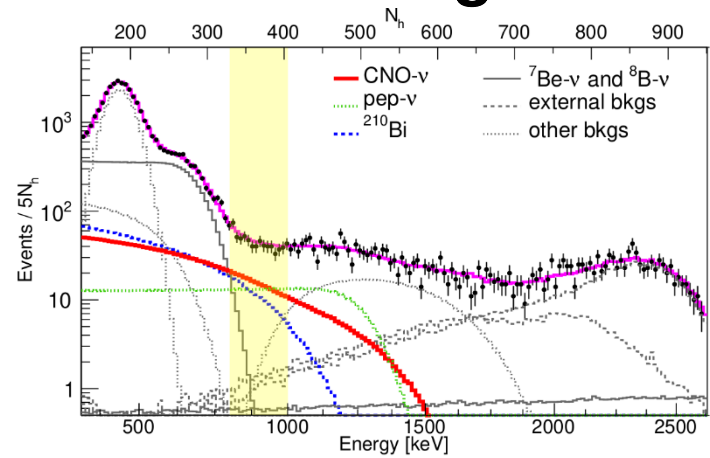

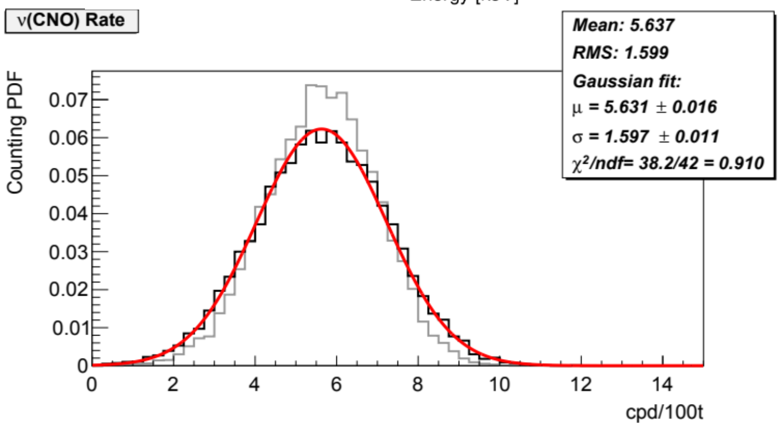

Systematics are obtained as the width of the distribution of the CNO rate after varying parameters on 10^4 Toy-MC realizations where we determine the number of CNO events by subtracting all the other species from the total events in the ROI.

$$R_{\nu(\mathrm{CNO})} = (5.6 \pm 1.6)\,\mathrm{cpd}/100\mathrm{t} \quad [\sim 3.5\,\sigma]$$

Consistent signal detection

The multivariate fit fully exploits all the information contained in the data and substantially enhances the CNO significance

Compendium of the results

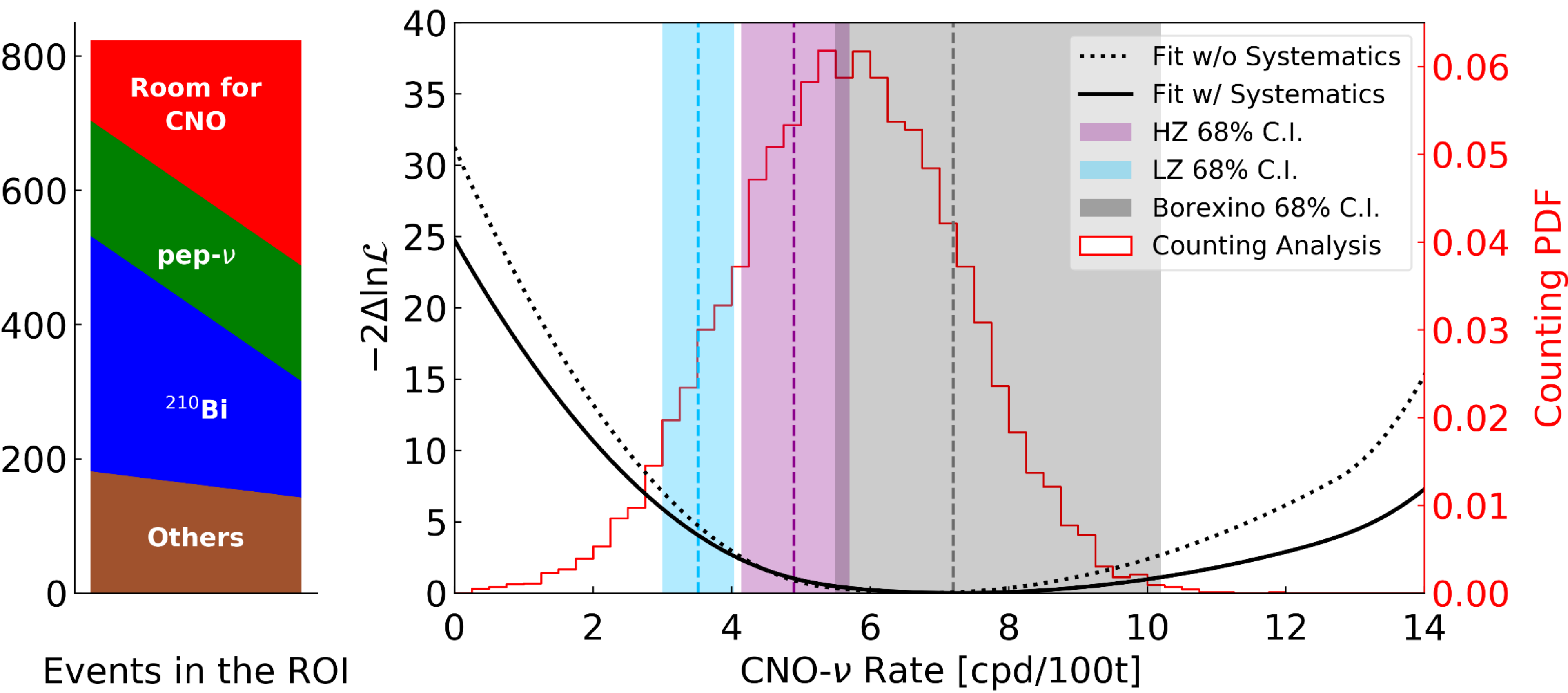

The enduring Borexino quest of the CNO neutrinos has finally produced the first observation of the signal

Conclusion

The undeterred, several years long effort to thermally stabilize the detector has resulted in the first detection of **CNO** neutrinos by Borexino

Significance of the detection **5 σ**

With this outcome Borexino has completely unraveled the two processes powering the Sun

the pp Chain and the **CNO Cycle**